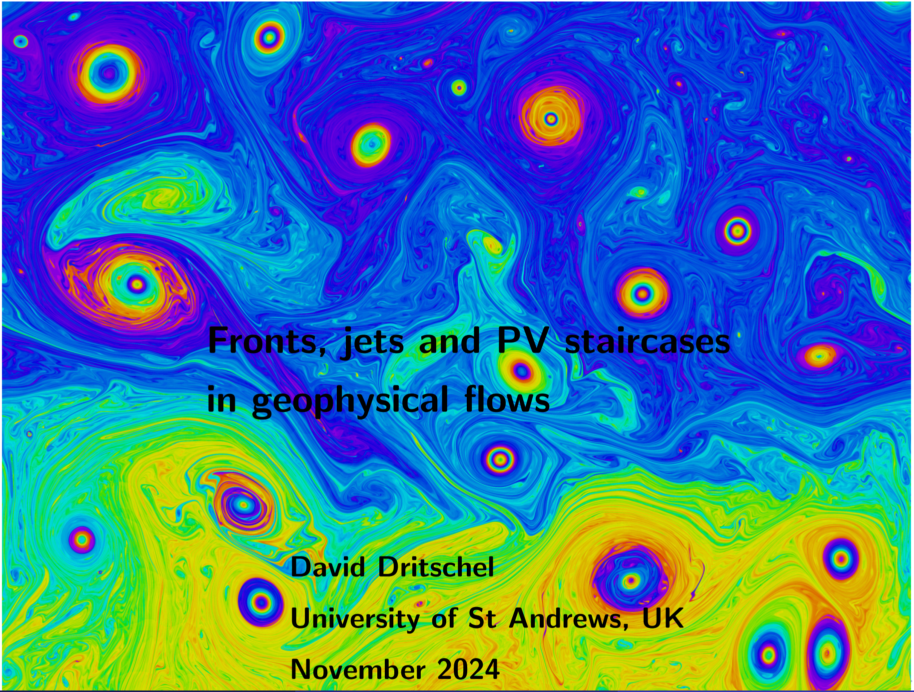

Fronts, jets and PV staircases in geophysical flows

David Dritschel
University of St Andrews, UK

November 2024

Outline

Potential Vorticity (PV) is often close to being a conservative dynamical tracer in many geophysical flows:

$$\frac{\mathrm{D}q}{\mathrm{D}t} \approx 0$$

JOURNAL OF GEOPHYSICAL RESEARCH, VOL. 99, NO. D1, PAGES 1071–1088, JANUARY 20, 1994

Transport out of the lower stratospheric Arctic vortex by Rossby wave breaking

D. W. Waugh,[1] R. A. Plumb,[1] R. J. Atkinson,[1] M. R. Schoeberl,[2] L. R. Lait,[2] P. A. Newman,[2] M. Loewenstein,[3] D. W. Toohey,[4] L. M. Avallone,[5] C. R. Webster,[6] and R. D. May[6]

Abstract. The fine-scale structure in lower stratospheric tracer transport during the period of the two Arctic Airborne Stratospheric Expeditions (January and February 1989; December 1991 to March 1992) is investigated using contour advection with surgery calculations. These calculations show that Rossby wave breaking is an ongoing occurrence during these periods and that air is ejected from the polar vortex in the form of long filamentary structures. There is good qualitative agreement between these filaments and measurements of chemical tracers taken aboard the NASA ER-2 aircraft.

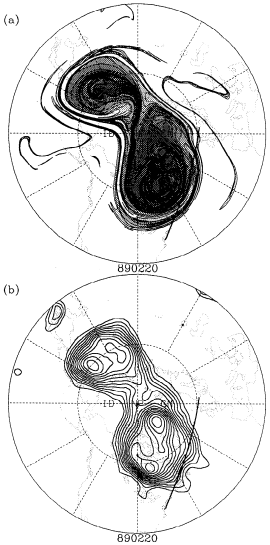

Figure 7. (a) Contours on February 20, 1989, from a 440 K CAS calculation starting 10 days earlier; (b) PV on the 440 K isentropic surface on February 20, 1989, from NMC analyses. Contour levels are as in Figure 5.

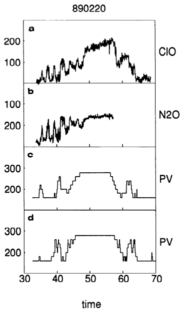

Figure 8. Data for ER-2 flight on February 20, 1989: (a) ClO (in parts per trillion by volume) and (b) N_2O (in parts per billion by volume) as measured aboard the ER-2, and PV from 440 K CAS calculation starting (c) 10 and (d) 20 days earlier. Potential temperature along flight is approximately 450 K.

On the February 21, 1989, flight from Wallops Island to Moffett Field, the flight path was outside the vortex, but according to the CAS calculation, it again crossed through surrounding filaments (see Figure 9). The filaments crossed contain air only from the very outer edge of the vortex. The chemical tracers on this flight again show fine-scale structure (Figure 10) and are consistent with the picture from CAS. Note that the peak N_2O values are characteristic of air at the very outer edge of the vortex. The agreement between the cross section from CAS and the chemical tracers is rather

Contours of PV are virtually *material contours*, meaning they carry the same fluid particles at all times (if q is conserved).

PV is not passive, but directly feeds back into the flow and largely controls the flow's dynamical and thermodynamical structure through 'PV inversion'.

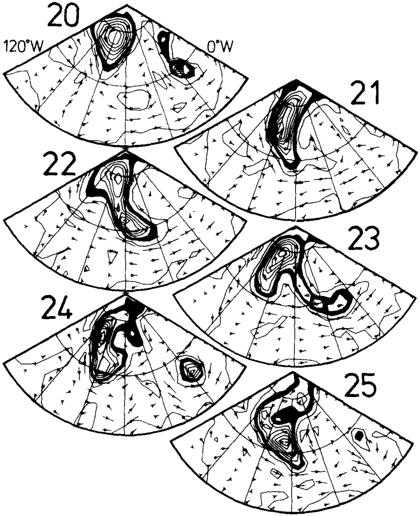

's of the 300 K IPV maps for the period 20–25 September 1982. The region (

Quart. J. R. Met. Soc. (1985), **111**, pp. 877–946

551.509.3:551.511.2:551.511.32

On the use and significance of isentropic potential vorticity maps

By B. J. HOSKINS[1], M. E. McINTYRE[2] and A. W. ROBERTSON[3]

Linear and nonlinear stability of monotonic PV

Rossby waves are manifestations of this PV inversion principle. Such waves owe their existence to gradients of PV.

The following sketch reminds us of the basic Rossby-wave mechanism:

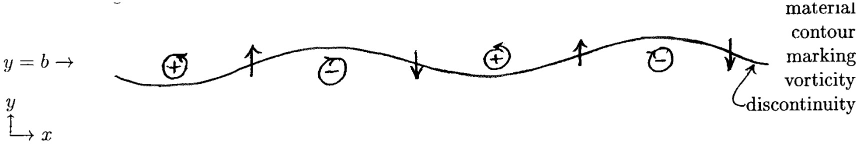

(From M.E. McIntyre's GEFD lecture notes).

- *Any PV contour* supports Rossby waves, even when it is a jump in PV.

- Moreover, *monotonic* distributions of PV (e.g. in latitude) are linearly stable, and even *nonlinearly stable* at least in the absence of gravity waves (Dritschel, *J. Fluid Mech.* **191**, 1988).

Rossby waves ... or Kelvin waves ... or Rayleigh waves

Consider the simplest situation of a vorticity interface at $y = \eta(x, t)$ separating two infinite, planar regions of uniform vorticity:

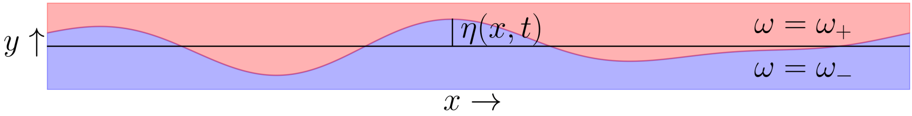

The flow is governed by the 2D Euler equations, which in vorticity form are

$$\frac{\mathrm{D}\omega}{\mathrm{D}t} = 0\,; \qquad \nabla^2\psi = \omega\,; \quad u = -\frac{\partial\psi}{\partial y}\,; \quad v = \frac{\partial\psi}{\partial x}\,.$$

The undisturbed basic-state is independent of x (and t), so since $\omega = \partial v/\partial x - \partial u/\partial y$, the flow is purely zonal:

$$u = \bar{u}(y) = -\omega_\pm y \quad \text{for} \quad \pm\, y > 0\,.$$

Linear analysis

We displace the interface from $y = 0$ to $y = \eta(x, t)$, where $\partial\eta/\partial x \ll 1$.

The vorticity remains uniform in the two regions. Hence, the perturbation streamfunction ψ' satisfies $\nabla^2\psi = 0$ in each region.
Taking $\eta(x, t) = \hat{\eta}\, e^{\mathrm{i}(kx-\sigma t)}$, then

$$\psi' = \hat{\psi}\, e^{-k|y|} e^{\mathrm{i}(kx-\sigma t)}$$

to leading order. This must be continuous at $y = 0$ since

$$v = \frac{\partial\psi}{\partial x} \quad \Rightarrow \quad v' = \mathrm{i}k\psi'$$

and v $(= v')$ must be continuous.

The interface is *material*: it moves with the fluid $\Rightarrow$

$$\frac{\mathrm{D}\eta}{\mathrm{D}t} = v(x, \eta, t) \quad \Rightarrow \quad -\mathrm{i}\sigma\hat{\eta} = \mathrm{i}k\hat{\psi}\,.$$

The total horizontal velocity $u = \bar{u} + u'$ must be continuous at $y = \eta \;\Rightarrow$

$$-\omega_{-}\eta + u'(x, 0^{-}, t) = -\omega_{+}\eta + u'(x, 0^{+}, t)$$

but

$$u' = -\frac{\partial \psi'}{\partial y} \quad \Rightarrow \quad u'(x, 0^{\pm}, t) = \pm k\hat{\psi}\, e^{\mathrm{i}(kx - \sigma t)}\,.$$

Hence, with $\Delta\omega \equiv \omega_{+} - \omega_{-}$, we find

$$\Delta\omega\,\hat{\eta} = 2k\hat{\psi}\,.$$

Previously, we found $-\sigma\hat{\eta} = k\hat{\psi}$, so eliminating $k\hat{\psi}$ we obtain

$$\sigma = -\tfrac{1}{2}\Delta\omega\,.$$

- Waves move left (westward) at constant speed $c = \omega/k = -\Delta\omega/(2k)$.

"Traditional" Rossby waves

Consider the 2D (single-layer) quasi-geostrophic model governed by

$$\frac{\mathrm{D}q}{\mathrm{D}t} = 0\,; \qquad \nabla^2\psi - k_{\mathrm{D}}^2\psi = q - \beta y\,; \quad u = -\frac{\partial\psi}{\partial y}\,; \quad v = \frac{\partial\psi}{\partial x}\,,$$

where $k_{\mathrm{D}} = L_{\mathrm{D}}^{-1} = f_0/\sqrt{gH}$ is the Rossby deformation wavenumber and β is the planetary vorticity gradient.

For a basic state at rest, $q = \bar{q}(y) = \beta y$ and $\psi = \bar{\psi} = 0$. Let $q = \bar{q} + q'$ where q' is sufficiently small to allow one to linearise the governing equations:

$$\frac{\partial q'}{\partial t} + \beta v' = 0\,; \qquad \nabla^2\psi' - k_{\mathrm{D}}^2\psi' = q'\,; \quad u' = -\frac{\partial\psi'}{\partial y}\,; \quad v' = \frac{\partial\psi'}{\partial x}\,.$$

These are *constant-coefficient* equations. Hence, we may seek plane-wave solutions,

$$\left\{q', \psi', u', v'\right\} = \left\{\hat{q}, \hat{\psi}, \hat{u}, \hat{v}\right\}\, e^{\mathrm{i}(kx+ly-\sigma t)}\,.$$

"Traditional" Rossby waves

This results in a set of algebraic equations,

$$-\mathrm{i}\sigma\hat{q} + \beta\hat{v} = 0\,; \quad -(k^2 + l^2 + k_{\mathrm{D}}^2)\hat{\psi} = \hat{q}\,; \quad \hat{u} = -\mathrm{i}l\hat{\psi}\,; \quad \hat{v} = \mathrm{i}k\hat{\psi}\,.$$

Non-trivial solutions (with $\hat{q} \neq 0$) require σ to take the values

$$\sigma = \frac{-\beta k}{k^2 + l^2 + k_{\mathrm{D}}^2}$$

for all wavenumbers k and l.

These waves also have a westward phase velocity, in this case $c = \omega/k = -\beta/(k^2 + l^2 + k_{\mathrm{D}}^2)$.

◇ ◇ ◇ ◇ ◇ ◇ ◇ ◇ ◇ ◇ ◇ ◇ ◇ ◇ ◇ ◇ ◇ ◇

Notably, *both* Rayleigh and Rossby waves are characterised by $c \to 0$ as $k \to \infty$: short waves become *non-dispersive*.
This is important for the nonlinear problem.

Time ↓

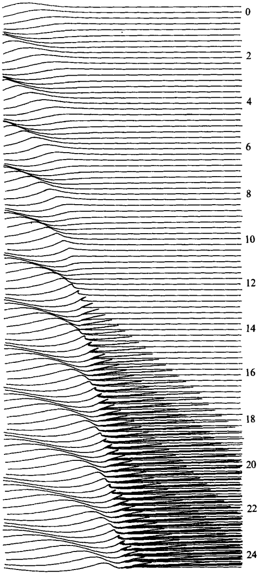

FIGURE 2. The evolution of an initially antisymmetric disturbance to a circular vortex on the plane

J. Fluid Mech. (1988), *vol.* 194, *pp.* 511–547
Printed in Great Britain

The repeated filamentation of two-dimensional vorticity interfaces

By DAVID G. DRITSCHEL
Department of Applied Mathematics and Theoretical Physics, University of Cambridge, Silver Street, Cambridge CB3 9EW, UK

(Received 20 May 1987 and in revised form 28 January 1988)

Undular disturbances of *arbitrarily small steepness* to the boundary of a circular patch of uniform vorticity are found to give way to a qualitatively different type of behaviour after a time inversely proportional to the initial wave steepness squared. Repeatedly, thin filaments are drawn out at a frequency of nearly half the vorticity jump across the interface (the intrinsic frequency of linear waves on the interface),

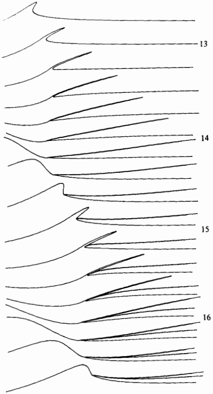

FIGURE 3. An enlarged view of part of figure 2 at the onset of filamentation, between $t = 12.75$ and 16.75.

Waves ***break***, even though *linearly stable*!

Of course, J and the A_i are conserved not only for the disturbed flow

$$y_i(x,t) = y_{ei} + \eta_i(x,t)$$

but also for the basic state y_{ei}, and, not surprisingly, any combination of these conserved quantities is likewise conserved. The particular combination

$$\mu = J - J_e - \sum_i \Delta Q_i \, y_{ei}(A_i - A_{ei})$$

$$= \tfrac{1}{2}\sum_i \Delta Q_i \oint_{C_i} \eta_i^2(x,t)\,\mathrm{d}x, \qquad (5)$$

is precisely quadratic in the disturbance, and, therefore, when all of the ΔQ_i have the same sign, $\|\eta\| = |\mu|^{\frac{1}{2}}$ qualifies as a norm, and we have

$$\|\eta\|(t) = \|\eta\|(0). \qquad (6)$$

This of course implies Liapunov stability, and indeed more. Not only does a sufficiently small initial disturbance imply boundedness for all time of the (same) norm, but the boundedness applies for an initial disturbance of any magnitude whatever.

The more general situation of a continuous vorticity distribution is straightforwardly obtained by taking the limit of an infinite number of contours; $\Delta Q_i \to \mathrm{d}Q$, $\eta_i(x,t) \to \eta(x,t;Q)$. The condition that the ΔQ_i all have the same sign becomes the requirement that the basic flow be monotonic. In this limit,

$$\|\eta\|^2 = \frac{1}{2}\int_{Q_{\min}}^{Q_{\max}} \mathrm{d}Q \oint \eta^2(x,t;Q)\,\mathrm{d}x. \qquad (7)$$

J. Fluid Mech. (1988), *vol.* 191, *pp.* 575–581
Printed in Great Britain

Nonlinear stability bounds for inviscid, two-dimensional, parallel or circular flows with monotonic vorticity, and the analogous three-dimensional quasi-geostrophic flows

By DAVID G. DRITSCHEL

Department of Applied Mathematics and Theoretical Physics, University of Cambridge, Silver Street, Cambridge CB3 9EW, UK

(Received 11 August 1987)

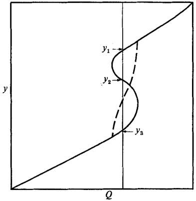

FIGURE 1. The basic flow ($y_e(Q)$, dashed line) corresponding to the disturbed initial condition ($Q(y)$, solid line) which minimizes the y-displacement norm while preserving vorticity measure.

Nonlinear stability *allows* Rossby wave breaking!

Non-monotonic PV profiles get *re-arranged* via *inhomogeneous PV mixing.*

The Rhines scale

So, nonlinear stability *does not prevent* Rossby wave breaking and subsequent mixing. *It only limits it.*

Wave steepening and breaking are *generic*, even for small perturbations to a rest state with $q = f_0 + \beta y$ or $q = 2\Omega \sin\phi$ (Scott & Dritschel, *Zonal Jets*, CUP 2019).

What sets the latitude or y scale of the mixing? Rhines (1975) argued that this is determined by a balance between the Rossby wave frequency and a typical turbulent eddy frequency:

$$\frac{\beta}{k} \sim k u_{\text{eddy}} \quad \Rightarrow \quad 1/k = \left(\frac{u_{\text{eddy}}}{\beta}\right)^{1/2} \equiv L_{\text{Rh}} \,,$$

known as the 'Rhines scale'. However, this assumes that the Rossby deformation length $L_{\text{D}} \gg L_{\text{Rh}}$, and does not account for forcing or damping.

Inhomogeneous mixing

McIntyre (1982) argued that this mixing must be *inhomogeneous*:
if the total PV variation is preserved,
the mixing must reduce gradients in some places,
and **increase** them in others.

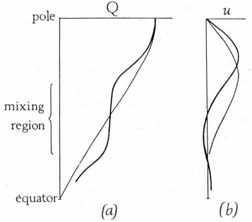

Figure 1: Schematic from McIntyre (1982), suggesting the robustness of nonlinear jet-sharpening by inhomogeneous PV mixing. Here most of the mixing is on the equatorward flank of an idealized stratospheric polar-night jet, in a broad midlatitude "surf zone" due to the breaking of Rossby waves arriving from below. The profiles can be thought of as giving a somewhat blurred, zonally-averaged picture. The

Where the PV gradients are steepened, eastward jets form by the PV inversion principle.

In between, in the mixed regions, there must be a westward return flow, by continuity.

Contour advection simulation of flow in a β channel for $L_{\mathrm{D}} \to \infty$

Shown is the PV field $q(\boldsymbol{x}, t)$ at a few times t.

From D & McIntyre, *JAS* 2008

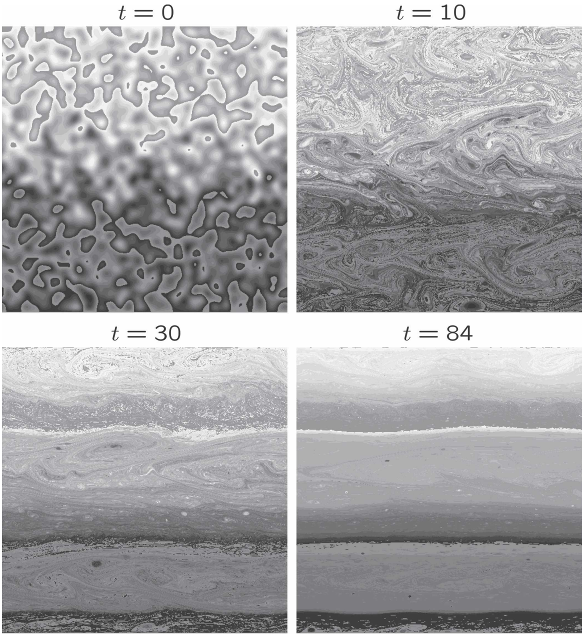

FIG. 5. Simulation of a quasigeostrophic shallow-water turbulent flow in a channel (see section 4). Time evolves to the right and downward, as labeled in units of $4\pi/|q'|_{\max}$. That is, the eddy turnaround time is unity for the initial maximum PV anomaly.

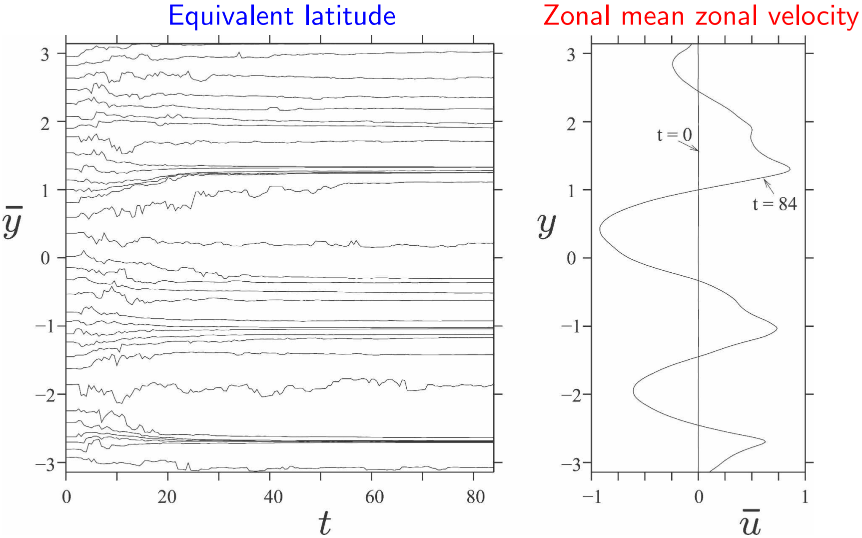

FIG. 6. Diagnostics for the experiment of Fig. 5. The left-hand panel shows the time evolution of the zonal-mean position $\bar{y}(q, t)$ of each PV contour that wraps the domain (i.e., that closes on itself only through the periodic boundaries $x = \pm\pi$). The latitudinal coordinate y is in units of L_D, and time t is in units of $4\pi/|q'|_{\max}$. PV mixing

For a single-layer quasi-geostrophic flow (illustrated above for $L_{\mathrm{D}} = 1$), PV inversion determines the zonal velocity u from

$$\nabla^2\psi - \psi/L_{\mathrm{D}}^2 = q - \beta y \qquad , \qquad u = -\partial\psi/\partial y \, .$$

For $q = q(y)$ in the form of one or several mixed zones — a PV staircase, $u(y)$ exhibits multiple eastward jets:

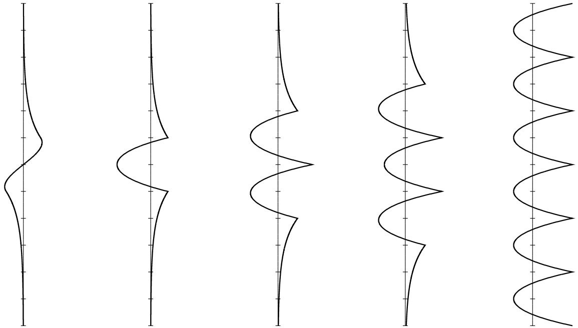

Figure 7: Idealized mass and velocity profiles for perfect staircase steps, as determined by PV inversion. Tick marks are at intervals of $y = b = L_{\mathrm{D}}$. From left to right, the first two profiles are for a single step or mixing zone, respectively the mass shift or surface-elevation change given by (5.2)ff. and the velocity profile given by (5.1)ff. The remaining profiles are the velocity profiles for two, three and an infinite number of perfect steps, the last from Eq. (5.3) shifted by b. Note that the angular

For a single mixed zone, $q = 0$ for $|y| < b$, one can show

$$\psi = \beta L_D^3 \left[k_D y - \mu \sinh(k_D y) \right] \quad \text{and} \quad u = \beta L_D^2 \left[-1 + \mu \cosh(k_D y) \right]$$

with adjoining exponential tails $\propto e^{-k_D |y|}$ for $|y| \geq b$.

Here, $\mu \equiv (1 + b k_D) e^{-b k_D}$ and $k_D = 1/L_D$ as before.

This is illustrated below for $\beta = 1$ and $b = 1$.

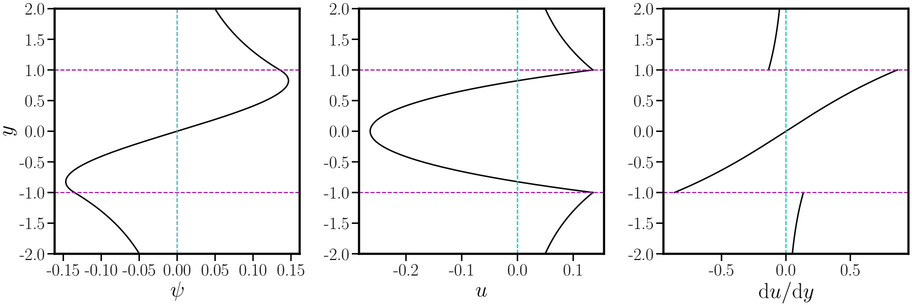

Notably, the **strongest** shear exists just inside the mixed zone.

Jet spacing and PV staircases

Here, the flow is strictly zonal — not turbulent — *yet* the Rhines scale

$$L_{\mathrm{Rh}} = \sqrt{u_{\mathrm{rms}}/\beta}$$

is proportional to the jet spacing, L_j, computed only by PV inversion:

$$L_j = 45^{1/4} L_{\mathrm{Rh}} \approx 2.59 L_{\mathrm{Rh}}$$

for $L_{\mathrm{D}} \to \infty$.

This closely agrees with what is found in full spherical geometry (Dunkerton & Scott, *JAS* 2008).

But how complete can PV mixing be? Incomplete mixing increases L_j/L_{Rh}.

- The Rhines scale alone does not predict jet spacing, even for $L_{\mathrm{D}} \to \infty$.

Jet sharpening by turbulent mixing

Dritschel & Scott, *Phil. Trans. R. Soc. A* **369** (2011) investigated the effect of turbulent mixing on an initially broad jet,

$$q(x,y,0) = \beta y + q_0'(y) \quad \text{with} \quad q_0'(y) = \pi\beta\,\mathrm{erf}(y/w)\,.$$

We add noise with an energy spectrum $\propto k^3 e^{-2\pi(k/k_0)^2}$ and amplitude $q'_{\mathrm{rms}} = 2\pi\beta q_e$. We take $w=1$, $\beta=2$ and a domain width & height of 2π.

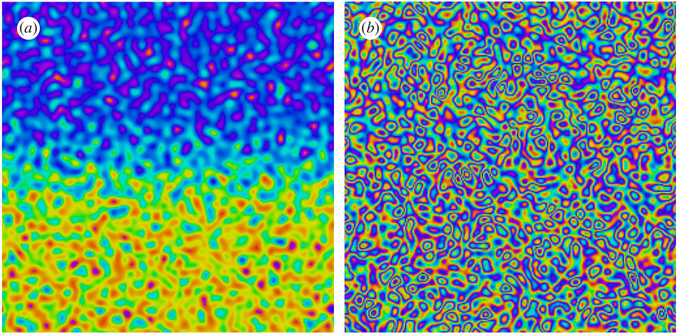

Figure 2. Initial PV field (basic state plus perturbation) for perturbation amplitudes (*a*) $q_e =$ 0.5 and (*b*) $q_e = 4$. (Online version in colour. The colour range from red through green/cyan to

Jet sharpening by turbulent mixing

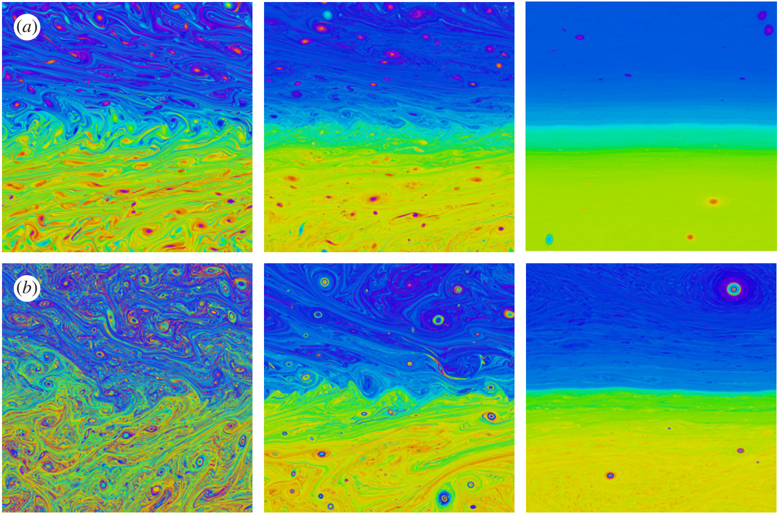

Figure 3. PV at times (i) $t = 5$, (ii) $t = 20$, (iii) $t = 200$ for the cases (a) $L_{\mathrm{D}}^{-1} = 0$ and $q_{\mathrm{e}} = 1$ and (b) $L_{D}^{-1} = 0$ and $q_{\mathrm{e}} = 4$; colours as in figure 2. (Online version in colour.)

Jet sharpening by turbulent mixing

The effect of finite deformation length. Here $L_\mathrm{D} = 1/4$.

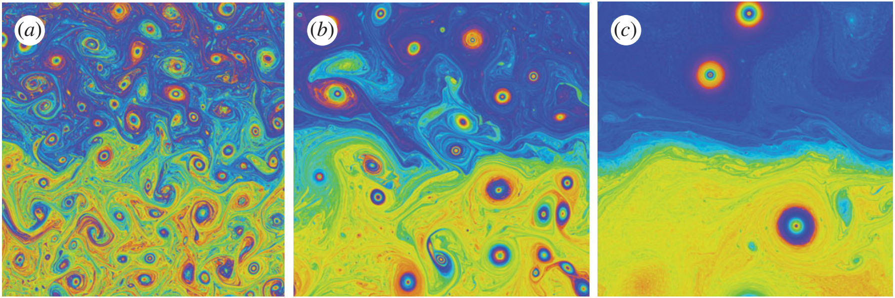

Figure 4. PV at times (a) $t = 10$, (b) $t = 40$, (c) $t = 400$ for the case $L_\mathrm{D}^{-1} = 4$ and $q_\mathrm{e} = 4$; colours as

The jet appears broader and wavier than in the case for $L_\mathrm{D} \to \infty$ (for the same perturbation amplitude q_e). Vortices are larger and more prevalent.

Jet sharpening by turbulent mixing

The effect of finite deformation length. Here $L_\mathrm{D} = 1/8$ — *even smaller.*

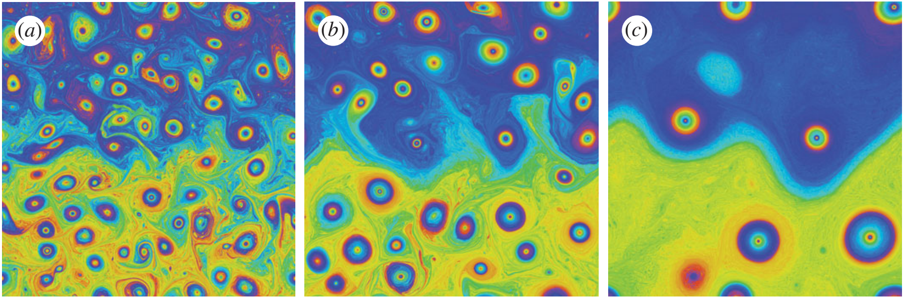

Figure 6. PV at times (a) $t = 25$, (b) $t = 100$, (c) $t = 1000$ for the case $L_\mathrm{D}^{-1} = 8$ and $q_\mathrm{e} = 4$; colours

The jet appears even broader and wavier, and vortices proliferate.

Jet sharpening by turbulent mixing: summary

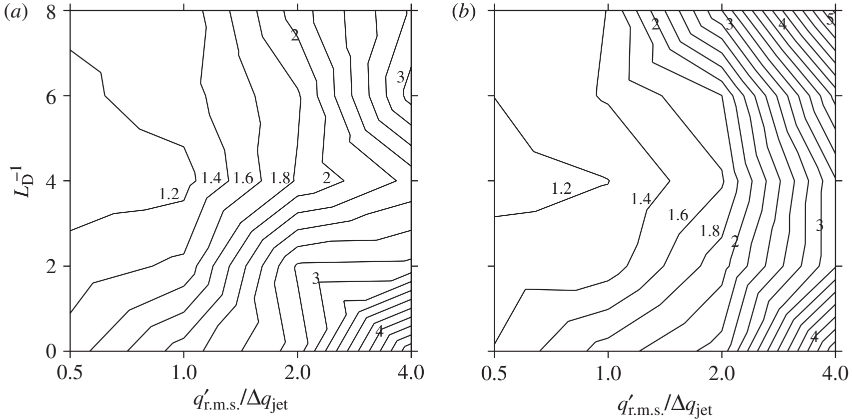

Figure 11. Jet-weighted averages of PV gradient for all calculations $q_e = 0.5, 1, 2, 4$ and $L_D^{-1} = 0, 2, 4, 6, 8$: (a) based on equivalent latitude $\langle \mathrm{d}q/\mathrm{d}y_e \rangle$ and (b) based on the zonal mean $\langle \mathrm{d}\bar{q}/\mathrm{d}y \rangle$. Values are normalized by the value of the corresponding basic state.

Forcing

In *forced* flows, there exists an additional length scale,

$$L_\varepsilon = (\varepsilon/\beta^3)^{1/5} \, ,$$

where ε is the rate of kinetic energy injection (Maltrud & Vallis, 1991). There may also be a separate forcing scale L_f.

What emerges depends on four length scales L_D, L_Rh, L_ε, L_f — if we assume that the domain scale is much larger *and* the dissipation scale is much smaller.

Scott & D *JFM* (2012) considered the simplest case for which $L_D \to \infty$. A linear damping, at rate r, is applied to the PV, i.e.

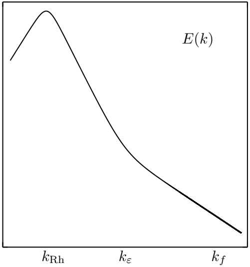

Figure 1.1 Schematic energy spectrum indicating the length scales $L_\mathrm{Rh} = k_\mathrm{Rh}^{-1}$, $L_\varepsilon = k_\varepsilon^{-1}$, and $L_f = k_f^{-1}$.

$$\frac{\mathrm{D}q}{\mathrm{D}t} = \mathcal{F} - r\zeta \quad \text{with} \quad \zeta = \nabla^2\psi \, ,$$

forcing $\mathcal{F}$, and damping $r \propto \varepsilon$ so that the energy equilibrates at $\mathcal{E} = \varepsilon/2r$.

Equilibrated flows (at $t = 10/r$) computed by Contour Advection (CLAM)

Here the PV anomaly $q - \beta y$ is shown

(a) $L_{\mathrm{Rh}}/L_{\varepsilon} = 3.0$

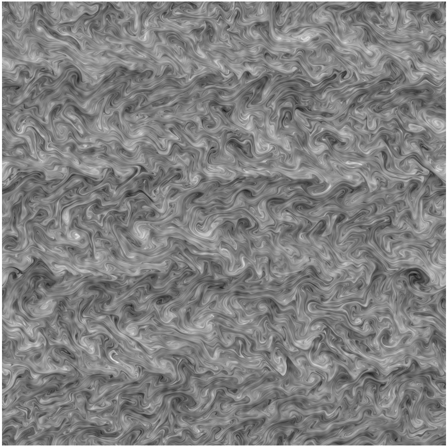

(b) $L_{\mathrm{Rh}}/L_{\varepsilon} = 10.8$

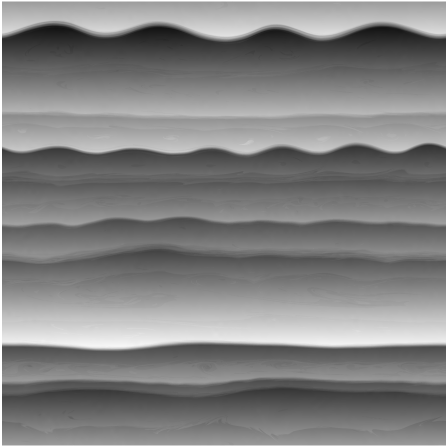

PV staircases emerge only for **large** $L_{\mathrm{Rh}}/L_{\varepsilon}$. *Note:* Rossby waves persist.

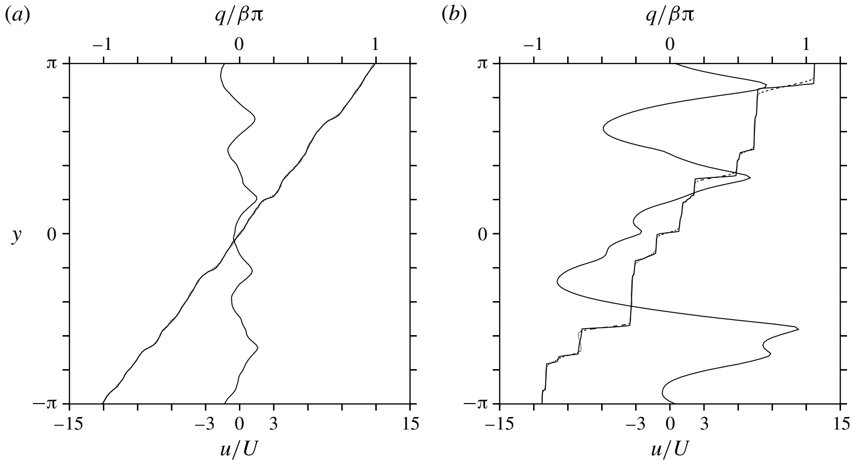

FIGURE 5. $\bar{u}(y)$ (solid line), $\bar{q}(y)$ (dotted line) and $q(y_e)$ (solid line) at $t = 10/r$ for the cases (*a*) $r = 256 \times 10^{-4}$ ($L_{Rh}/L_\varepsilon = 3.0$) and (*b*) $r = 1 \times 10^{-4}$ ($L_{Rh}/L_\varepsilon = 10.8$, corresponding to figure 3(*a*,*d*). Velocities are scaled by $U = \sqrt{\varepsilon_0/r}$.

Corresponding mean profiles of q and u, from Scott & D, *JFM* 2012.

How close can one get to a *perfect* staircase? *very!*

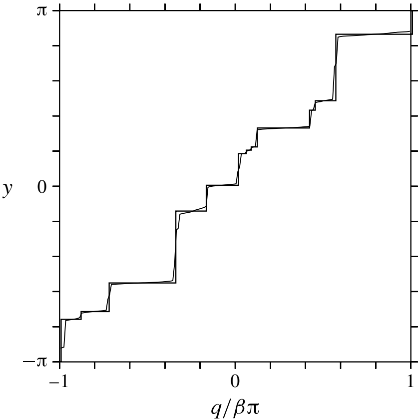

FIGURE 12. The profile $q(y_e)$ from the case of physical-space forcing and $r = 0.0001$ ($L_{Rh}/L_\varepsilon = 10.8$, see figure 5*b*) together with a notional staircase constructed as described in the text.

Weak, **large-scale** topographic forcing also creates PV staircases, here without damping.

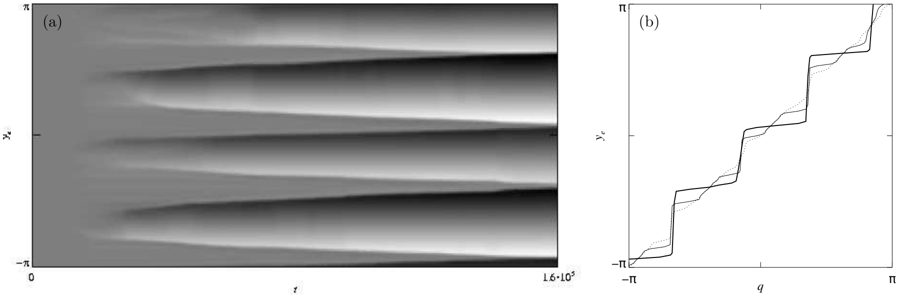

configuration at any instant it so may not be determined *a priori*. Here, the value of ε used in L_ε is at any time approximated by the average energy input rate measured

Figure 1.5 (a) Time evolution of equivalent latitude potential vorticity anomaly, $q(y_e, t) - \beta y_e$ for topographic forcing amplitude $a_0 = 0.004$. (b) Profile of $q(y_e)$ at $t = 32000$, $t = 64000$ and $t = 160000$ ($L_{\mathrm{Rh}}/L_f = 1.0$, $L_{\mathrm{Rh}}/L_\varepsilon = 11.0$ at the final time).

From Scott & D, *Zonal Jets* 2019

(a) $t = 4000$ (b) $t = 8000$

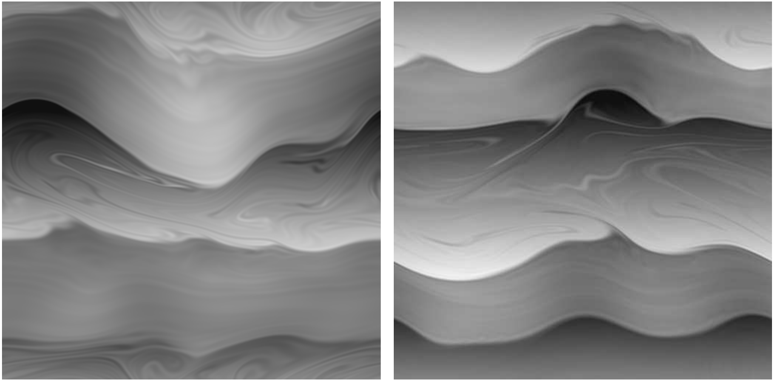

This is illustrated next in a few characteristic numerical simulations from an extensive set spanning a wide pa-

Figure 1.6 $q(x, y)$ at $t = 4000$ (a) and $t = 8000$ (b) for topographic forcing amplitude $a_0 = 0.016$; values of $L_{\mathrm{Rh}}/L_{\varepsilon}$ are 5.3 6.0, respectively.

Zonal averages clearly smear out the staircase structure

Small Rossby deformation length

When the Rossby deformation length L_D is finite and smaller than L_{Rh}, *things get more interesting....*

(a) $L_{\mathrm{Rh}}/L_D = 1/4$ (b) $L_{\mathrm{Rh}}/L_D = 1$ (c) $L_{\mathrm{Rh}}/L_D = 4$

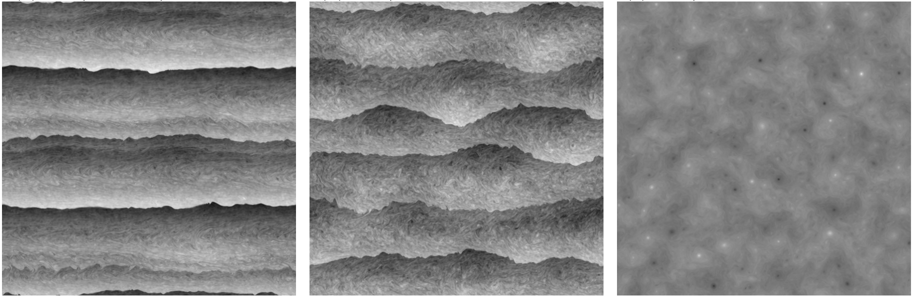

PV anomaly $q - \beta y$ at $t = 10/r$, for small-scale forcing and weak damping.

As L_{Rh}/L_D increases, jets get more wavy ... then *disappear?*

The jets have not disappeared ... they are just different.

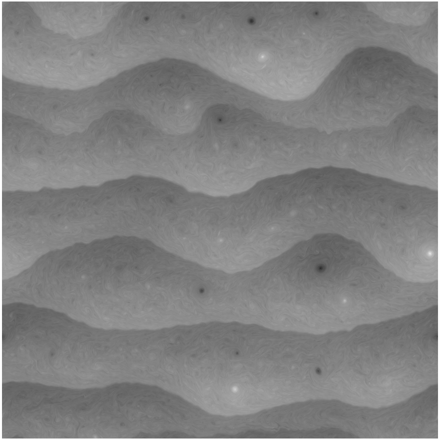

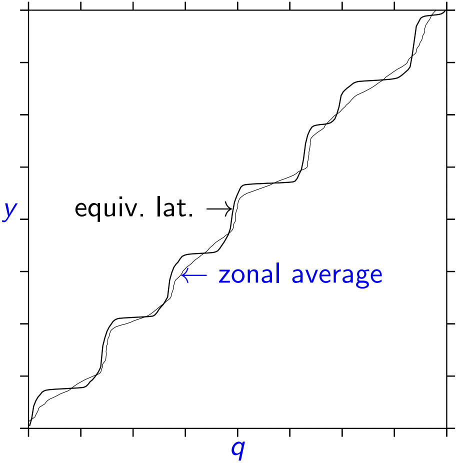

Now vortices and closed ring jets are prevalent

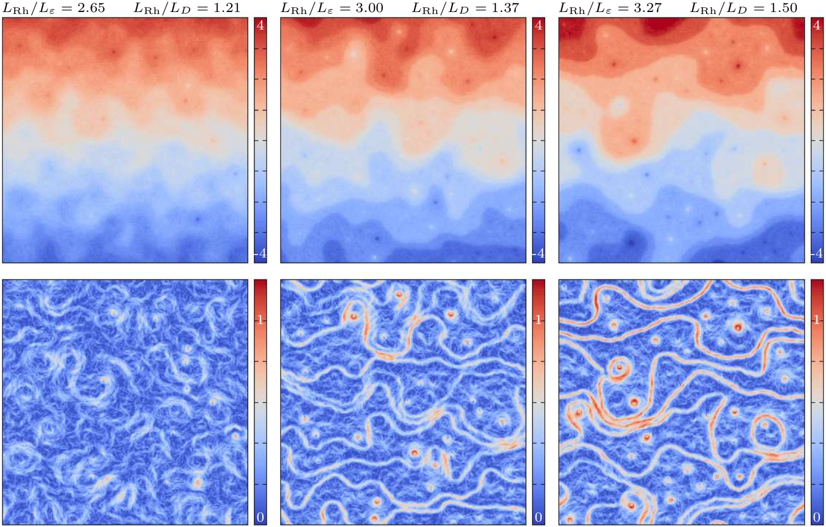

FIGURE 3. Snapshots of the potential vorticity (top row) and speed (bottom row) from the simulation with $n = -1$, at values of $L_{\mathrm{Rh}}/L_\varepsilon$ and L_{Rh}/L_D as indicated in the figure.

Persistent, weak energy injection sharpens the staircase (from Scott, Burgess & D, *J. Fluid Mech.* **930**, A20, 2022).

Oceanic jets — small L_{D} phenomena?

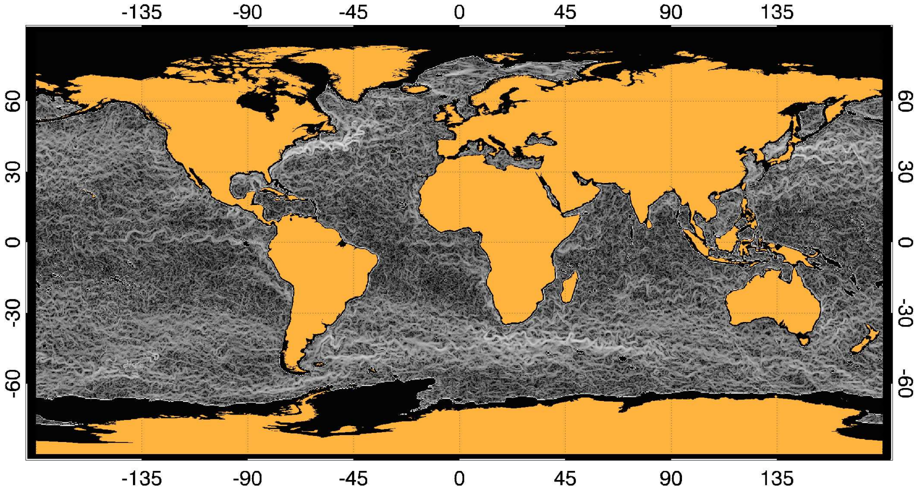

Topographically-forced shallow-water flows on a sphere

Relative vorticity ζ at three times; top: narrow band, bottom: broad band

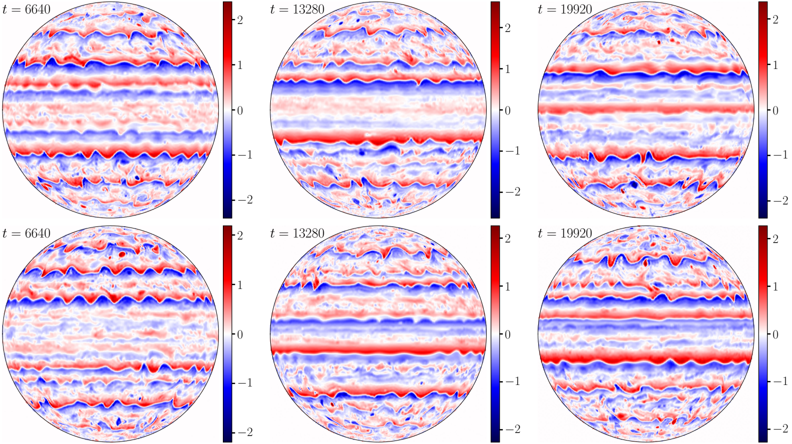

From Dritschel, Jalali & Scott, *in preparation*;
see also Scott & Polvani, *J. Atmos. Sci* (2008).

J. Fluid Mech. (2019), *vol.* 866, R3, doi:10.1017/jfm.2019.133

JFM RAPIDS
journals.cambridge.org/rapids

Long frontal waves and dynamic scaling in freely evolving equivalent barotropic flow

B. H. Burgess[1,†] and D. G. Dritschel[1]

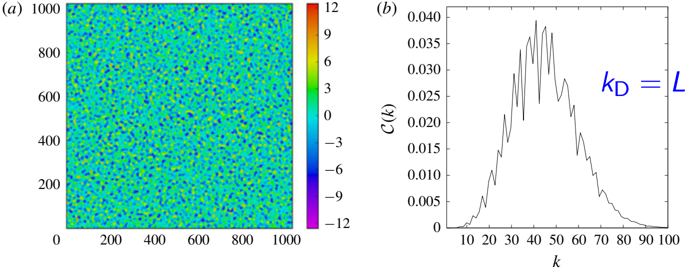

$k_D = L_D^{-1} = 40$

$\beta = 0$

FIGURE 1. (*a*) Initial PV field and (*b*) spectrum $\mathcal{C}(k)$ as defined in (2.1).

Jets emerge as well ... they just surround patches of PV

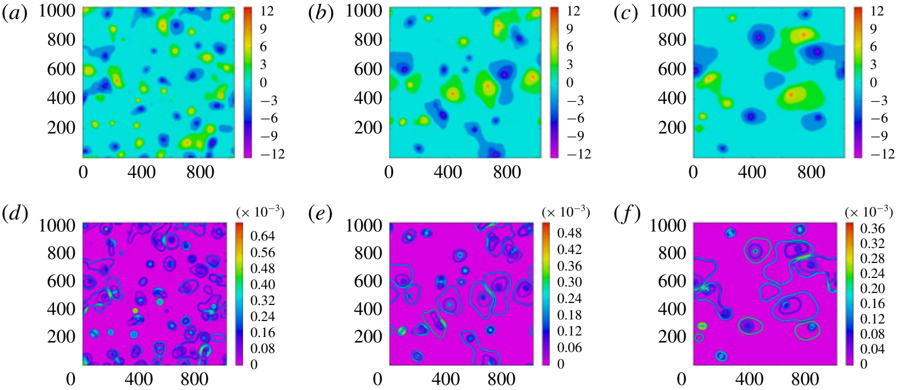

FIGURE 4. (*a*–*c*) PV fields and (*d*–*f*) corresponding kinetic energy density fields. (*a*) PV field at $t = 27\,000$, (*b*) PV field at $t = 125\,000$, (*c*) PV field at $t = 343\,000$, (*d*) KE field at $t = 27\,000$, (*e*) KE field at $t = 125\,000$, (*f*) KE field at $t = 343\,000$.

The PV takes on a 'wedding cake' structure — a staircase!

PV measure: area A occupied by PV above a given threshold

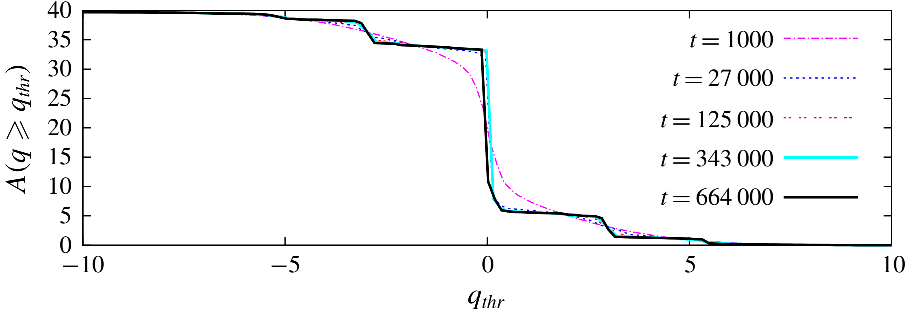

With time, the PV becomes progressively well mixed *between* sharp fronts — the jets.

J. Fluid Mech. (2015), *vol.* 783, *pp.* 1–22.
doi:10.1017/jfm.2015.535

On the late-time behaviour of a bounded, inviscid two-dimensional flow

David G. Dritschel[1,†], Wanming Qi[2,3,4] and J. B. Marston[3,4]

Staircases even form in the other extreme: $L_{\mathrm{D}} \to \infty$ and $\beta = 0$

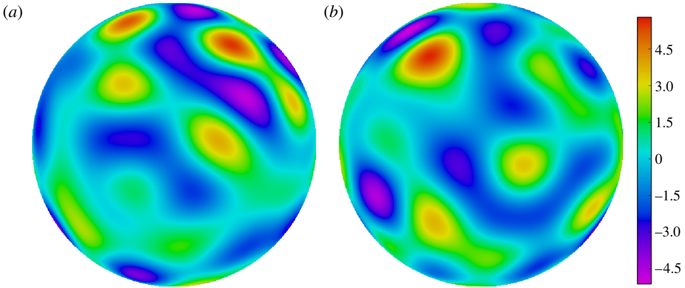

Initial conditions: a superposition of low degree spherical harmonics

$\omega(\lambda, \phi, t = 4000)$

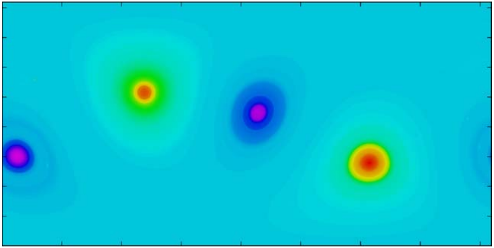

Vortex cross sections

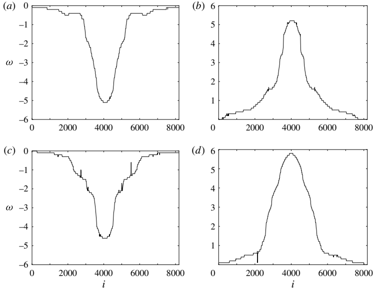

FIGURE 8. (*a*–*d*) Constant-latitude cross-sections of the vorticity field taken through each of the four large-scale vortices (from left to right in figure 6*d*) in the highest-resolution CLAM simulation at $t = 4000$. The relative longitudinal grid point i is indicated on the

Each vortex exhibits a stepped profile, *the result of inhomogeneous mixing*

J. Fluid Mech. (2017), *vol.* 816, *pp.* 586–618. © Cambridge University Press 2017 586
doi:10.1017/jfm.2017.79

On the energetics of a two-layer baroclinic flow

Thibault Jougla[1,†] and David G. Dritschel[1]

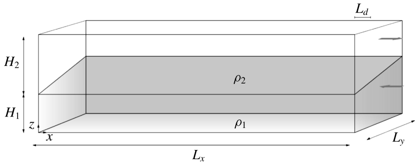

FIGURE 2. Illustration of the initial undisturbed state of a two-layer quasi-geostrophic vertically sheared flow, with uniform westward flow in the lower layer and uniform eastward flow in the upper layer.

Early work: Panetta, *JAS* 1993

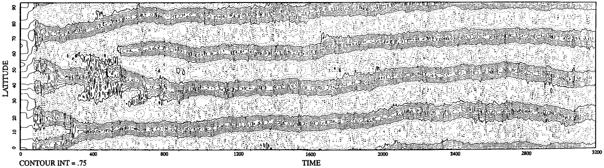

FIG. 10. Zonally averaged upper-layer transient eddy zonal flow in long experiment, as a function of meridional distance in Rossby radii (ordinate) and time (abscissa: 0–3200).

$t = 3000$ days

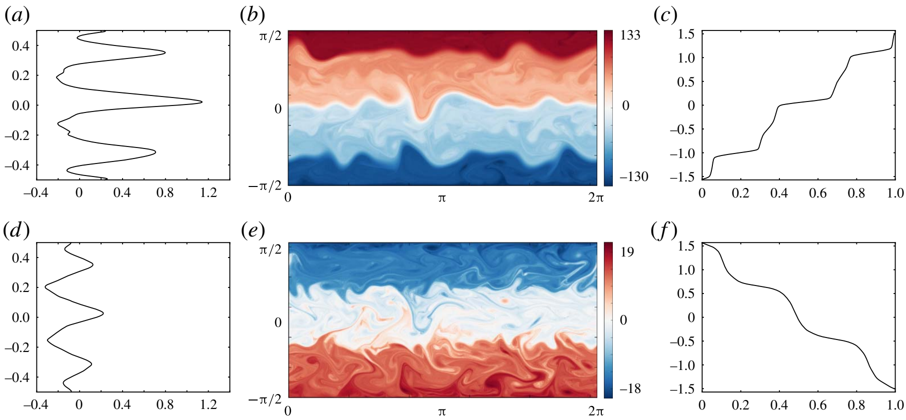

FIGURE 3. (Colour online) (*a–c*) The upper layer flow, and (*d–f*) the lower layer flow, all at $t = 3000$. (*a,d*) Normalised latitude $2y/\pi$ versus zonally averaged zonal velocity $\bar{u}_i(y, t)$. (*b,e*) PV field $q_i(x, y, t)$ over the entire domain. (*c,f*) Equivalent latitude $y_e(\tilde{q}, t)$ versus normalised PV $\tilde{q} = (q - q_{min})/(q_{max} - q_{min})$.

$t = 4000$ days: turbulent phase (baroclinic instability)

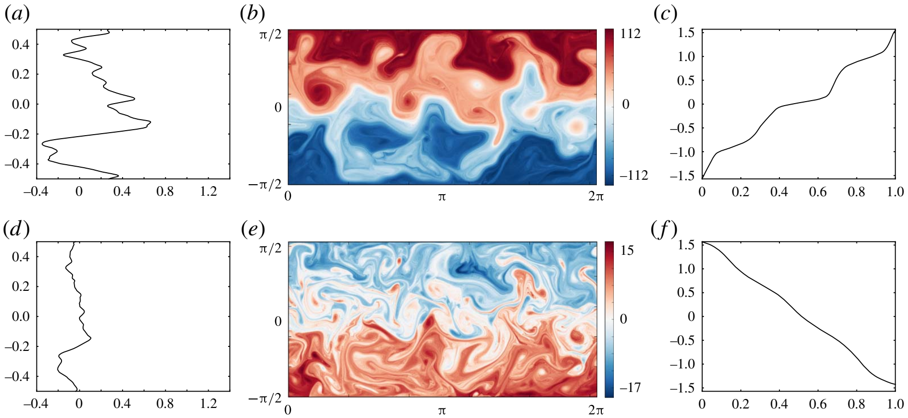

FIGURE 4. (Colour online) (*a*–*c*) The upper layer flow, and (*d*–*f*) the lower layer flow, all at $t = 4000$. (*a*,*d*) Normalised latitude versus zonally averaged zonal velocity (note that plot scales for u are the same as in figure 3). (*b*,*e*) PV field over the entire domain. (*c*,*f*) Equivalent latitude $y_e(\tilde{q}, t)$ versus normalised PV.

$t = 9400$ days: quiescent phase

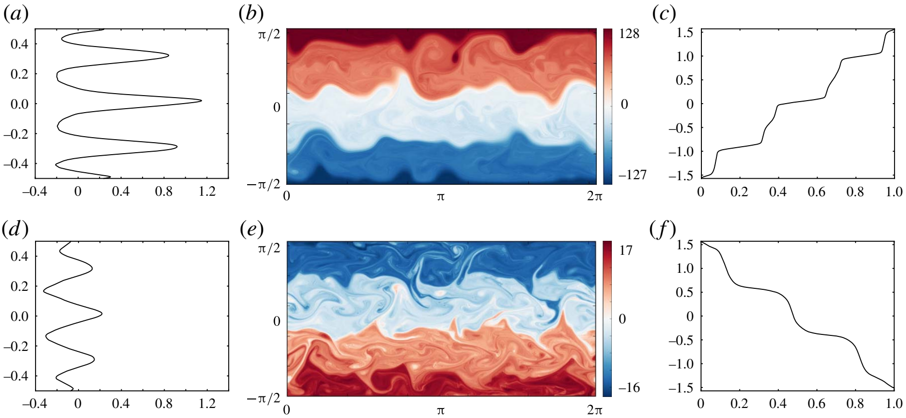

FIGURE 5. (Colour online) (*a–c*) The upper layer flow, and (*d–f*) the lower layer flow, all at $t = 9400$. (*a*,*d*) Normalised latitude versus zonally averaged zonal velocity (note that plot scales for u are the same as in figure 3). (*b*,*e*) PV field over the entire domain. (*c*,*f*) Equivalent latitude $y_e(\tilde{q}, t)$ versus normalised PV.

Recipé for jet formation in atmospheres and oceans

The *essential* ingredient required for jet formation is **irreversible**, *nonlinear* Rossby wave breaking.

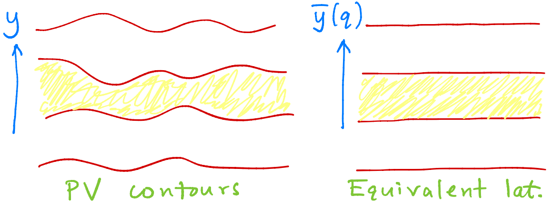

Jet formation *cannot* occur in linear theory: *it is not a linear process*.

The mathematical proof is simple:

Under linear dynamics, the mean position of each potential vorticity (PV) contour (the equivalent latitude) can never change in time.

Thus, the area between PV contours can never change and mean PV gradients are preserved — a simple consequence of PV conservation.

Shear induces wave breaking: waves break into the region of greatest shear. Subsequently, PV filaments are rapidly stretched and mixed there.

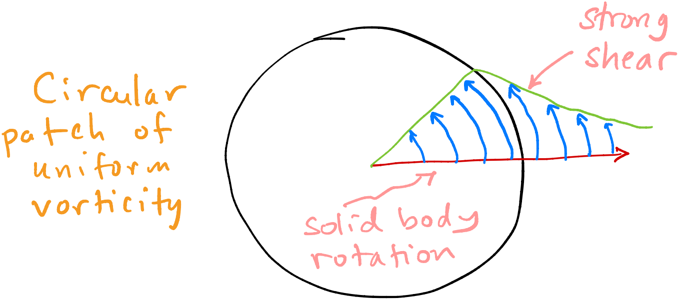

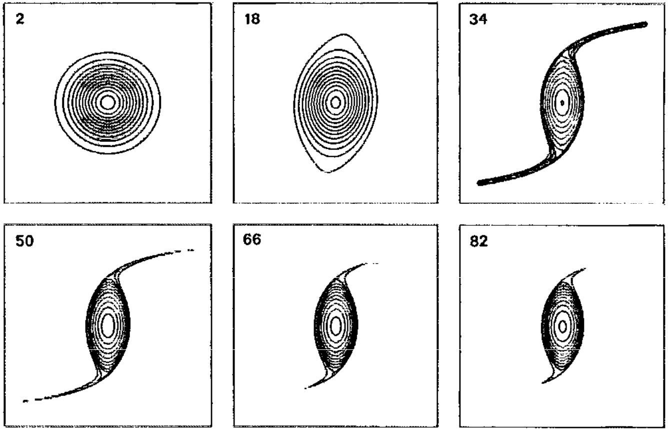

FIG. 2. Quasi-adiabatic evolution of the Gaussian vortex submitted to external adverse shear (strain parameter $\hat{\gamma}=0.05$, Re=8000). This figure shows a 4.32×4.32 box centered in the $2\pi\times2\pi$ computational domain. Times 2, 18, 34, 50, 66, and 82 as indicated in the frames.

(From Mariotti, Legras & D, *Phys. Fluids* **6(12)**, 1994 — vortex stripping)

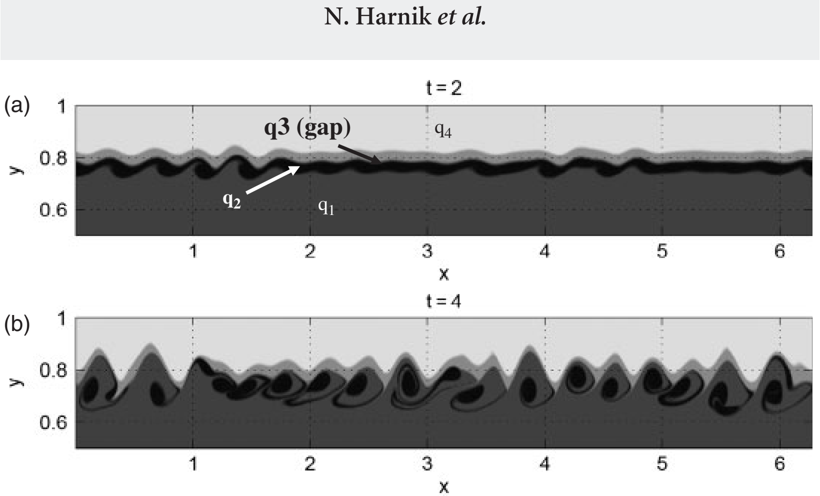

(From Harnik, D & Heifetz, *QJRMS* **(140)**, 2014 — "On the equilibration of asymmetric barotropic instability")

... a bit later

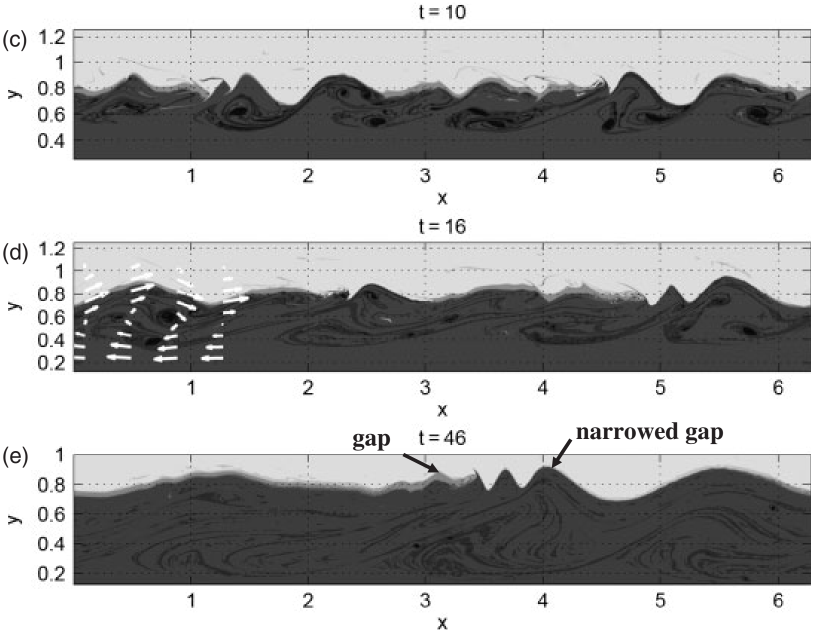

t = 10
(c)
1.2
1
0.8
0.6
0.4
y
1
2
3
4
5
6
x
t = 16
(d)
1.2
1
0.8
0.6
0.4
0.2
y
1
2
3
4
5
6
x
gap
t = 46
narrowed gap
(e)
1
0.8
0.6
0.4
0.2
y
1
2
3
4
5
6
x

Wave breaking now occurs on *both* sides of the jet, into regions of **strong** shear.

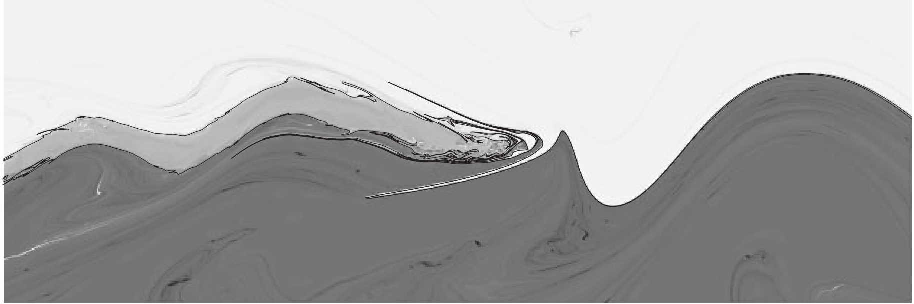

The gap region of light grey PV has virtually disappeared on the right, leading to *extremely sharp* PV gradients.

The positive feedback mechanism

Wave breaking occurs preferentially in regions of reduced mean PV gradients.

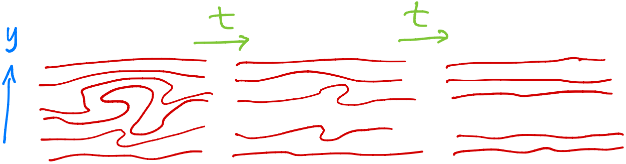

This implies there is a positive feedback mechanism: mixing further weakens mean gradients in places, while strengthening them in others, forming jets (inhomogeneous PV mixing).

This process is only limited by available perturbations to the mean flow. Without forcing, these diminish as eddies transfer their kinetic energy to the mean flow and become insufficient to induce further wave breaking and mixing.

Shear: the universal mechanism?

Fundamentally, *shear induces wave breaking*.

Consider a single *passive* PV contour located initially at $y = \eta(x, 0)$ $= F(x)$ in the shear flow $u = \Lambda y$.

Since $\mathrm{D}y/\mathrm{D}t = v = 0$, then $y = \eta(x, t)$ satisfies *Burgers equation:*

$$\frac{\partial \eta}{\partial t} + \Lambda \eta \frac{\partial \eta}{\partial x} = 0.$$

The (implicit) solution is $\eta(x, t) = F(x - \Lambda \eta t)$, which becomes multi-valued at $t = 1/(\Lambda F'_{\mathrm{max}})$: *the wave breaks.*

Now suppose that the PV contour is active, i.e. has a PV jump of Δq across it. Now the PV contour oscillates, protecting itself from shear, *at least if* $\Delta q \gtrsim \Lambda$.

Shear: the universal mechanism?

Otherwise, when $\Delta q \lesssim \Lambda$, *the contour breaks and mixes.*

Its mean position moves toward lower shear, or toward another PV contour, in both cases so that $\Delta q \gtrsim \Lambda$.

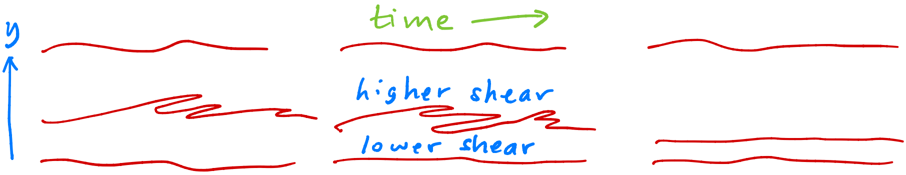

PV contours closely approach to **augment** their effective Δq and therefore protect them from shear.

Weak jets established early on provide (part of) the source of this shear — initially weak. They **strengthen** by attracting nearby PV contours, which then weakens PV gradients between jets.

A superposition of two offset staircases shows the shear reduction between closer PV contours (dashed):

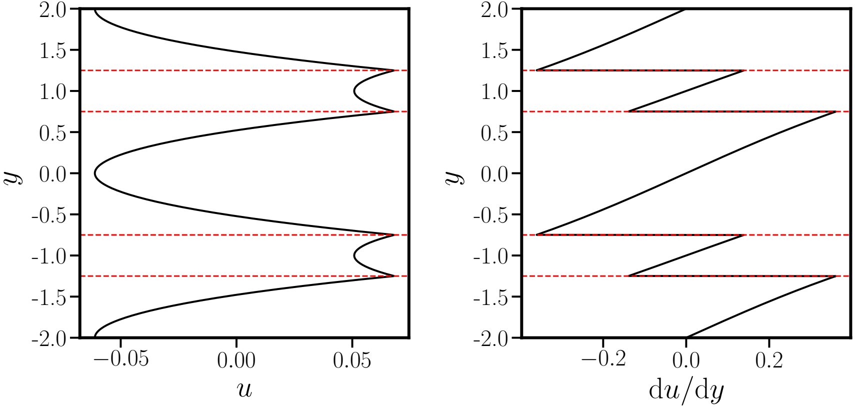

Exact result for quasi-geostrophic flow when $\Delta q = 0.5$ and $L_D = 1$; adapted from D & McIntyre *JAS* 2008

Conclusions, part 1 of 2

Potential vorticity (PV) is a key dynamical tracer in atmospheric and oceanic dynamics; it is often advection dominated — i.e. nearly conserved following fluid particles.

PV inversion, alongside balance relations, enables one to deduce both dynamical and thermodynamical fields *from a single scalar tracer,* often to astonishing accuracy.

PV advection is fundamentally *nonlinear*; PV largely induces the flow that advects it.

PV contours — indeed *any* PV variation — support Rossby waves. However, nonlinearity generically induces wave breaking.

Conclusions, part 2 of 2

Wave breaking on PV contours leads to *inhomogeneous mixing*, weakening PV gradients in some places, *but* strengthening PV gradients in others, *giving rise to eastward jets.*

Such mixing can lead to PV staircases in remarkably diverse flows:
• forced/unforced, • small/large L_{D}, • small-scale/large-scale forcing (of many varieties), • barotropic/baroclinic, *etc.*

PV mixing, or homogenisation, causes strong shear to develop at the edges of the mixed zones. This shear is a consequence of PV inversion.

Shear efficiently mixes PV in zones, leaving sharp PV steps on their boundaries. Such steps are co-located with *jets* by PV inversion.